Inorganic Chemistry

Article

pubs.acs.org/IC

New Polar Intermetallic Phases RE_2Zn_5Tt (RE = La–Nd; Tt = Sn and Pb): Synthesis, Structure, Chemical Bonding, and Magnetic Properties

Nian-Tzu Suen and Svilen Bobev*

Department of Chemistry and Biochemistry, University of Delaware, Newark, Delaware 19716, United States

Supporting Information

ABSTRACT: Reported are the synthesis, crystal structure, electronic structure, and magnetic properties of a series of zinc-rich ternary phases with formulas RE_2Zn_5Tt (RE = La–Nd; Tt = Sn and Pb). The structures of these compounds have been established by single-crystal and powder X-ray diffraction. They crystallize in the orthorhombic space group *Cmcm* (No. 63, $LaRhSn_2$ structure type, Pearson symbol oC32). The most prominent structural feature is the trigonal-planar coordination of the Sn(Pb) atoms; the latter interconnect layers of Zn atoms to comprise a complex $[Zn_5Tt]$ polyanionic framework. The structural relationships between the structure of the title compounds and the $EuIn_4$, La_3Al_{11}, and $YIrGe_2$ structure types are highlighted. Temperature-dependent DC magnetization measurements indicate Pauli-like paramagnetism for La_2Zn_5Sn, while Ce_2Zn_5Sn, Pr_2Zn_5Sn, and Nd_2Zn_5Sn display Curie–Weiss behavior in the high-temperature regime. At cryogenic temperatures, the magnetic responses of Ce_2Zn_5Sn, Pr_2Zn_5Sn, and Nd_2Zn_5Sn appear to deviate from the Curie–Weiss law; however, no magnetic orderings could be observed down to 5 K. Theoretical considerations of the electronic structure on the basis of the tight-binding linear muffin-tin orbital (TB-LMTO-ASA) method are also presented and discussed.

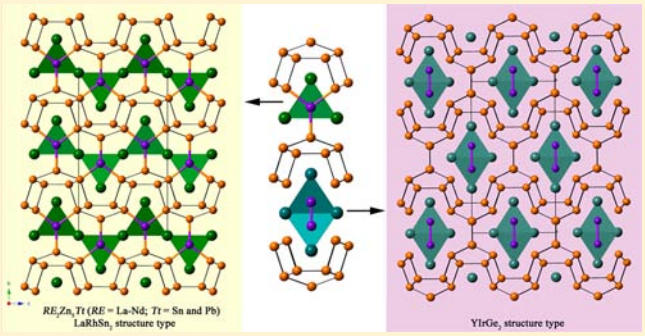

INTRODUCTION

Polar intermetallic compounds can be regarded as a bridge between the typical intermetallics and the typical Zintl phases, since they bear resemblance to both classes, in terms of chemical bonding.[1] In the Zintl phases, for instance, because of the closed-shell electronic configurations, the bonding within the polyanions can usually be associated with the covalent two-center two-electrons bonds, while the interactions between the cations and the anions are thought to be ionic.[2] Polar intermetallics are very much akin to the Zintl phases in that regard, except that the degree of polarization is not as extreme, and the "cations" contribute significantly to the overall bonding as well—they do not just take the role of "spectators" or "electron donors".[3]

Polar intermetallics provide excellent opportunities to investigate the relationships between structures, physical properties, and electronic structures. For instance, there are almost 2000 phases that adopt the tetragonal $BaAl_4$ structure type (and/or its ordered ternary variants $ThCr_2Si_2$ and $CaBe_2Ge_2$).[4] The electronic structure of $BaAl_4$ has been studied by Zheng and Hoffman,[5] and by Miller and Burdett,[6] who have shown it to be most stable with 14 valence electrons per formula. Nevertheless, it is also known that the valence electrons in this structure can be varied between 12 and 16, which indicates that factors beyond the electron count are at play here.[7] This is also evident from the fact that $CaAl_4$ and $EuIn_4$ form with structures, which can be recognized as distorted derivates of $BaAl_4$ (despite the same number of valence electrons being present for all three cases).[8] Another isoelectronic, but not isotypic, example is La_3Al_{11} (equivalent to $LaAl_{3.67}$),[9] which forms as a variant of $BaAl_4$ with ordered "vacancies". All these findings attest for the strong correlation between the crystal and electronic structure here, and in polar intermetallics in general.

Our previous work on ternary rare-earth metal germanides has shown remarkable structural diversity—take, for example, the series RE_2MgGe_2,[10] $(RE_{1-x}Mg_x)_5Ge_4$,[11] $RE_4Mg_7Ge_6$,[12] and $RE_4Mg_5Ge_6$[12]—all crystallizing with their unique bonding arrangements. Over the course of studying these compounds, we naturally became interested in the heavier tetrels (Tt = a group 14 element hereafter), as well as the RE–Zn–Tt systems; after all, Mg and Zn have similar atomic sizes/oxidation states.[13] Because of that, Zn chemistry is expected to mimic Mg chemistry, and it is not surprising that we, and others, have already found some isotypic phases.[12,14] However, many of the Zn-containing tetrelides should be noted for displaying more-complicated bonding patterns, arising from the versatile nature of the Zn–Zn interactions.[15] In this paper, we present the synthesis and the structural characterization of a new series of such zinc-rich ternary intermetallic phases with formulas RE_2Zn_5Tt (RE = La–Nd; Tt = Sn and Pb). Structural

Received: May 28, 2013
Published: July 17, 2013

   dx.doi.org/10.1021/ic401339v | *Inorg. Chem.* 2013, 52, 9102–9110

Table 1. Crystallographic Data and Refinement Parameters of RE_2Zn_5Sn (RE = La−Nd)

	La_2Zn_5Sn	Ce_2Zn_5Sn	Pr_2Zn_5Sn	Nd_2Zn_5Sn
fw, g mol^{-1}	723.36	725.78	727.36	734.02
crystal system	orthorhombic			
space group	*Cmcm* (No. 63), *Z* = 4			
λ, Å	0.71073			
T, K	200(2)			
a, Å	4.5508(8)	4.5047(14)	4.4756(5)	4.4494(15)
b, Å	16.753(3)	16.638(5)	16.5640(18)	16.510(6)
c, Å	9.1342(16)	9.104(3)	9.0747(10)	9.066(3)
V, Å^3	696.4(2)	682.3(4)	672.74(13)	666.0(4)
ρ_{calcd}, g cm^{-3}	6.899	7.065	7.181	7.320
μ (Mo Kα), cm^{-1}	322.9	337.7	352.1	365.2
GOF on F^2	1.141	1.147	1.117	1.082
R_1 [$I > 2\sigma(I)$]^a	0.0259	0.0153	0.0154	0.0274
wR_2 [$I > 2\sigma(I)$]^a	0.0542	0.0300	0.0360	0.0596
R_1 [all data]^a	0.0348	0.0171	0.0184	0.0394
wR_2 [all data]^a	0.0568	0.0305	0.0374	0.0648

$^aR_1 = \sum||F_0| - |F_c||/\sum|F_0|$; $wR_2 = [\sum[w(F_0^2 - F_c^2)^2]/\sum[w(F_0^2)^2]]^{1/2}$, and $w = 1/[\sigma^2F_0^2 + (A\cdot P)^2 + B\cdot P]$, $P = (F_0^2 + 2F_c^2)/3$; *A* and *B* are weight coefficients.

Table 2. Crystallographic Data and Refinement Parameters of RE_2Zn_5Pb (RE = La−Nd)

	La_2Zn_5Pb	Ce_2Zn_5Pb	Pr_2Zn_5Pb	Nd_2Zn_5Pb
fw, g mol^{-1}	811.86	814.28	815.86	822.52
crystal system	orthorhombic			
space group	*Cmcm* (No. 63), *Z* = 4			
λ, Å	0.71073			
T, K	200(2)			
a, Å	4.5550(4)	4.5140(12)	4.4636(8)	4.4594(8)
b, Å	16.8373(15)	16.751(4)	16.632(3)	16.622(3)
c, Å	9.1721(8)	9.159(2)	9.1240(16)	9.1187(17)
V, Å^3	703.44(11)	692.6(3)	677.4(2)	675.9(2)
ρ_{calcd}, g cm^{-3}	7.67	7.81	8.00	8.08
μ (Mo Kα), cm^{-1}	523.1	539.5	561.0	571.7
GOF on F^2	1.104	1.112	1.156	1.126
R_1 [$I > 2\sigma(I)$]^a	0.0251	0.0204	0.0204	0.0254
wR_2 [$I > 2\sigma(I)$]^a	0.0570	0.0392	0.0361	0.0513
R_1 [all data]^a	0.0259	0.0250	0.0223	0.0298
wR_2 [all data]^a	0.0575	0.0404	0.0365	0.0525

$^aR_1 = \sum||F_0| - |F_c||/\sum|F_0|$; $wR_2 = [\sum[w(F_0^2 - F_c^2)^2]/\sum[w(F_0^2)^2]]^{1/2}$, and $w = 1/[\sigma^2F_0^2 + (A\cdot P)^2 + B\cdot P]$, $P = (F_0^2 + 2F_c^2)/3$; *A* and *B* are weight coefficients.

relationships with the $EuIn_4$,[8b] La_3Al_{11},[9] and $YIrGe_2$[16] structure types are also discussed.

EXPERIMENTAL SECTION

Synthesis. The starting materials were purchased from common chemical vendors, and then they were stored and handled inside an argon-filled glovebox in order to prevent their deterioration from moisture and oxygen. Rare-earth metals (ingots, 99.9% from Ames Laboratory) and Sn (shot), Pb (ingot), and Zn (shot)—all from Alfa-Aesar or Acros with stated purities of >99.99%—were used as-received. The title compounds were first synthesized by fusing together the respective elements in Nb containers, which had been sealed in both ends with an arc-welder. To avoid oxidation, the Nb containers were enclosed in evacuated fused silica jackets (ca. 10^{-5} Torr). The reactions were carried out at 1173 K (heating rate of 200 K/h) for 12 h, followed by cooling to 1073 K over a period of 20 h, after which they cooled to room temperature by taking them out of the furnace. RE_2Zn_5Tt (RE = La−Nd; Tt = Sn and Pb) formed as irregular crystals that were brittle and had a metallic luster. They were mixed with some binary or ternary compounds such as RE_3Zn_{11},[17] $RE_{13}Zn_{58}$,[18] RE_3Zn_{22},[19] and/or REZnSn (YPtAs structure type).[20]

After the structure and composition of RE_2Zn_5Tt (RE = La−Nd; Tt = Sn and Pb) were established by single-crystal X-ray diffraction (XRD) data, new reactions with the correct stoichiometry were carried out. Although the desired phases were the major products, minor impurity phases were still apparent from the powder XRD patterns. This prompted us to explore different synthetic approaches, and one of them—a two-step route at lower temperature offered the highest purity samples. For this purpose, a pellet of the respective elements (in powder form, ground to a homogeneous mixture) was pressed and transferred into a silica tube, which was then connected to a vacuum line. After evacuation and flame sealing, the ampule was placed in a tube furnace and heated to 773 K at a rate of 200 K/h and kept for 24 h. Following this initial process, the pellet was air-cooled, ground into fine powder (in the glovebox), and pressed into a pellet again. Then, the new sample was equilibrated at 1073 K for 4 days. Powder XRD patterns revealed the final product to be almost-phase-pure RE_2Zn_5Tt (RE = La−Nd; Tt = Sn and Pb) with small amount of Sn or Pb left over. Growing crystals from Zn, Sn, or Pb fluxes was also attempted, and although small crystals could be obtained, the reactions' products were always contaminated with crystals from other phases.

Subsequent to the work on the stannide and plumbide compounds, we then moved to the corresponding germanide and silicide systems.

dx.doi.org/10.1021/ic401339v | Inorg. Chem. 2013, 52, 9102−9110

We also looked at reactions with the heavier rare-earth metals. These synthetic efforts were not successful and we could not produce the targeted phases. Instead, mixtures of $RE(Zn_{1-x}Ge_x)_2$ (α-$ThSi_2$ structure type) and another, yet unidentified phase were the main products, combined with the typical binary RE_3Zn_{11},[17] $RE_{13}Zn_{58}$,[18] and RE_3Zn_{22}[19] impurities.

Powder X-ray Diffraction. Powder XRD data were taken at room temperature on a Rigaku MiniFlex powder diffractometer with Cu Kα radiation. The powder XRD patterns of RE_2Zn_5Tt (RE = La–Nd; Tt = Sn and Pb) can be readily indexed and the peak positions/intensities matched the simulations (on the basis of the single-crystal X-ray work). The powder XRD patterns also indicated that the title compounds are stable in air for at least one month. A representative powder XRD pattern of La_2Zn_5Sn showing the calculated and the observed intensities is provided in the Supporting Information.

Single-Crystal X-ray Diffraction. Single-crystal XRD data were collected on a Bruker SMART CCD-based diffractometer equipped with a monochromated Mo Kα sealed-tube source. Crystals were selected under an optical microscope, cut to desired dimensions (<ca. 100 μm), and mounted on glass fibers with Paratone-N oil. Preliminary rotation images were acquired to access the crystal quality. After that, full spheres of data were collected in four batch runs with a frame width of 0.4° for ω and θ. Data collection and data integration were done using SMART[21] and SAINTplus[22] programs, respectively. Semiempirical absorption correction based on equivalent reflections was applied using SADABS.[23] The structures were solved by direct methods and refined to convergence by full matrix least-squares on F^2, as implemented in SHELXL.[24] Refined parameters include the scale factors, extinction coefficients, and the atomic positions (Structure TIDY standardized[25]) with the corresponding anisotropic displacement parameters. Relevant details of the crystallographic work for La_2Zn_5Sn, Ce_2Zn_5Sn, Pr_2Zn_5Sn, and Nd_2Zn_5Sn are summarized in Table 1; the structure solution and refinement parameters for La_2Zn_5Pb, Ce_2Zn_5Pb, Pr_2Zn_5Pb, and Nd_2Zn_5Pb are listed in Table 2, respectively. Final positional and equivalent isotropic displacement parameters are listed in Tables 3 and 4. Selected interatomic distances for La_2Zn_5Sn and La_2Zn_5Pb are tabulated in Table 5. The crystallographic information file (CIF) has also been deposited with Fachinformationszentrum Karlsruhe, 76344 Eggenstein, Leopoldshafen, Germany; fax: (49) 7247-808-666; E-mail: crysdata@fiz.karlsruhe.de; with depository numbers CSD-426183 for La_2Zn_5Sn, CSD-426182 for Ce_2Zn_5Sn, CSD-426181 for Pr_2Zn_5Sn, CSD-426180 for Nd_2Zn_5Sn, CSD-426179 for La_2Zn_5Pb, CSD-426178 for Ce_2Zn_5Pb, CSD-426177 for Pr_2Zn_5Pb, CSD-426176 for Nd_2Zn_5Pb.

Magnetic Susceptibility Measurements. Field-cooled (FC) direct current (DC) magnetic susceptibility measurements were carried out using a Physical Property Measurement System (PPMS). The magnetization (M) measurements were performed in the interval from 5 K to 300 K in an applied magnetic field (H) of 3 kOe. The RE_2Zn_5Sn samples (polycrystalline form, typically ca. 100 mg) were loaded in gel caps and secured with cotton to prevent them from moving under the magnetic field. The raw magnetization data were corrected for the holder contribution and converted to molar susceptibility ($\chi_m = M/H$). The net effective moments and Weiss temperatures were calculated from linear fit of the inversed magnetic susceptibility versus temperature. For the La_2Zn_5Sn sample, the measurements data were also acquired under a low applied field of 100 Oe to test the material for possible superconductivity.

Electronic Structure Calculations. To interrogate the chemical bonding, the electronic band structures of La_2Zn_5Sn and La_2Zn_5Pb were computed with the Stuttgart TB-LMTO 4.7 program.[26] The total and partial density of states (DOS and PDOS, respectively) and Crystal Orbital Hamiltonian Populations (COHP)[27] of selected atomic interactions are presented herein. The local density approximation (LDA) was used to treat exchange and correlation.[28] No empty spheres were needed to meet the minimum overlapping criteria. The symmetry of the potential was considered spherical inside each Wigner–Seitz (WS) sphere,[29] and a combined correction was used to take into account the overlapping part. The radii of WS spheres were determined by an automatic procedure and were as follows: La = 2.19–2.22 Å, Zn = 1.41–1.49 Å, Sn = 1.66 Å, and Pb = 1.69 Å. The basis sets included 6s, 6p, 5d, and 4f orbitals for La; 4s, 4p, and 3d orbitals for Zn; and 5s, 5p, and 5d orbitals for Sn (6s, 6p and 6d, and 5f orbitals for Pb). The La 6p, Zn 3d, Sn 5d, and Pb 6d and 5f orbitals were treated by the Löwdin downfolding technique.[29] The k-space integrations were made using the tetrahedron method, and the self-consistent charge density was obtained with 172 irreducible k-points in the Brillouin zone.

Table 3. Atomic Coordinates and Equivalent Isotropic Displacement Parameters (U_{eq}[a]) for RE_2Zn_5Sn (RE = La–Nd)

atom	Wyckoff site	x	y	z	U_{eq} (Å^2)
			La_2Zn_5Sn		
La1	4c	0	0.79365(5)	1/4	0.006(1)
La2	4a	0	0	0	0.009(1)
Sn1	4c	0	0.44323(7)	1/4	0.008(1)
Zn1	8f	0	0.18519(8)	0.1087(1)	0.010(1)
Zn2	8f	0	0.34410(8)	0.0152(1)	0.010(1)
Zn3	4c	0	0.6021(1)	1/4	0.014(1)
			Ce_2Zn_5Sn		
Ce1	4c	0	0.79454(3)	1/4	0.005(1)
Ce2	4a	0	0	0	0.007(1)
Sn1	4c	0	0.44396(3)	1/4	0.006(1)
Zn1	8f	0	0.18546(4)	0.10810(7)	0.007(1)
Zn2	8f	0	0.34409(4)	0.01622(7)	0.008(1)
Zn3	4c	0	0.60342(6)	1/4	0.012(1)
			Pr_2Zn_5Sn		
Pr1	4c	0	0.79501(3)	1/4	0.006(1)
Pr2	4a	0	0	0	0.008(1)
Sn1	4c	0	0.44456(3)	1/4	0.007(1)
Zn1	8f	0	0.18568(4)	0.10857(8)	0.009(1)
Zn2	8f	0	0.34375(4)	0.01666(8)	0.009(1)
Zn3	4c	0	0.60430(6)	1/4	0.012(1)
			Nd_2Zn_5Sn		
Nd1	4c	0	0.79598(5)	1/4	0.007(1)
Nd2	4a	0	0	0	0.009(1)
Sn1	4c	0	0.44534(7)	1/4	0.008(1)
Zn1	8f	0	0.18592(9)	0.1085(2)	0.009(1)
Zn2	8f	0	0.34439(9)	0.0174(4)	0.010(1)
Zn3	4c	0	0.6051(1)	1/4	0.015(1)

[a] U_{eq} is defined as one-third of the trace of the orthogonalized U^{ij} tensor.

RESULTS AND DISCUSSION

Structure. All title compounds are isoelectronic and isostructural, crystallizing in the orthorhombic space group $Cmcm$ (Pearson symbol $oC32$; see Tables 1 and 2), and a schematic representation of the structure is shown in Figure 1. For the sake of conciseness, the detailed discussion of the crystal and the electronic structure will be focused on La_2Zn_5Sn and La_2Zn_5Pb as representatives of the entire RE_2Zn_5Tt (RE = La–Nd; Tt = Sn and Pb) family.

There are six crystallographic sites in the asymmetric unit (Tables 3 and 4): two for the rare-earth metals, three for the Zn atoms, and one for the tetrel atom (Sn or Pb). The structure is devoid of disorder and all atom sites are fully occupied. Based on the crystallographic notations, this structure should be described with the $LaRhSn_2$ structure type,[30] where the positions of two rare-earth metals are the same for La_2Zn_5Sn and $LaRhSn_2$ (equivalent to $La_2Rh_2Sn_4$), while the Rh site in the latter is taken by Zn2 in the former (see Figure S1 in the

dx.doi.org/10.1021/ic401339v | Inorg. Chem. 2013, 52, 9102–9110

Table 4. Atomic Coordinates and Equivalent Isotropic Displacement Parameters (U_{eq})[a] for RE_2Zn_5Pb (RE = La–Nd)

atom	Wyckoff Site	x	y	z	U_{eq} (Å^2)
			La_2Zn_5Pb		
La1	4*c*	0	0.79410(5)	1/4	0.007(1)
La2	4*a*	0	0	0	0.010(1)
Pb1	4*c*	0	0.44414(3)	1/4	0.012(1)
Zn1	8*f*	0	0.18537(8)	0.1085(1)	0.011(1)
Zn2	8*f*	0	0.34295(8)	0.0139(1)	0.011(1)
Zn3	4*c*	0	0.6041(1)	1/4	0.016(1)
			Ce_2Zn_5Pb		
Ce1	4*c*	0	0.79491(5)	1/4	0.008(1)
Ce2	4*a*	0	0	0	0.011(1)
Pb1	4*c*	0	0.44513(3)	1/4	0.009(1)
Zn1	8*f*	0	0.18485(7)	0.1090(1)	0.009(1)
Zn2	8*f*	0	0.34224(8)	0.0146(1)	0.012(1)
Zn3	4*c*	0	0.6061(1)	1/4	0.020(1)
			Pr_2Zn_5Pb		
Pr1	4*c*	0	0.79629(5)	1/4	0.006(1)
Pr2	4*a*	0	0	0	0.008(1)
Pb1	4*c*	0	0.44644(3)	1/4	0.008(1)
Zn1	8*f*	0	0.18528(7)	0.1091(1)	0.008(1)
Zn2	8*f*	0	0.34219(7)	0.0160(1)	0.011(1)
Zn3	4*c*	0	0.6078(1)	1/4	0.017(1)
			Nd_2Zn_5Pb		
Nd1	4*c*	0	0.79623(6)	1/4	0.007(1)
Nd2	4*a*	0	0	0	0.009(1)
Pb1	4*c*	0	0.44645(4)	1/4	0.008(1)
Zn1	8*f*	0	0.18524(9)	0.1089(1)	0.008(1)
Zn2	8*f*	0	0.34238(9)	0.0157(1)	0.011(1)
Zn3	4*c*	0	0.6077(1)	1/4	0.016(1)

[a] U_{eq} is defined as one-third of the trace of the orthogonalized U^{ij} tensor.

Supporting Information). The La_2Zn_5Sn structure (Figure 1) can be viewed as a 3D framework of Zn and Sn atoms and La atoms occupying the channels within it. The polyanionic substructure is composed of corrugated Zn slabs, stacked in a direction of the crystallographic *b*-axis. They are "stitched" together via Sn or Pb atoms in nearly-perfect trigonal-planar fashion, which is a highly unusual coordination mode for a tetrel element.

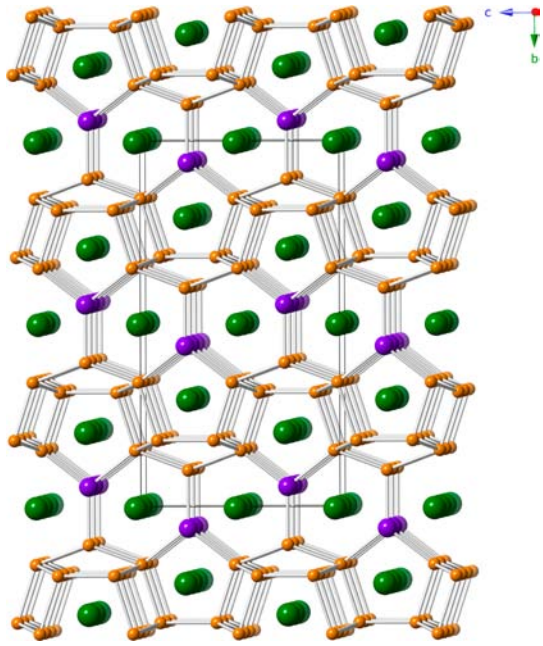

Figure 1. Schematic representation of the orthorhombic structure of La_2Zn_5Sn approximately along the [100] direction. The La atoms are shown as green spheres, and the Zn atoms are drawn as orange spheres, respectively. The Sn atoms are colored in purple.

Each Zn-only fragment features six-membered Zn_6 rings (Figure 2a), which have the "boat" shape instead of being planar. The corresponding Zn–Zn distances fall into very narrow ranges: 2.582(3)–2.5881(9) Å in La_2Zn_5Sn, and 2.5834(9)–2.596(3) Å in La_2Zn_5Pb (see Table 5). The six-

Table 5. Important Interatomic Distances and Their Integrated COHP Values (−*i*COHP) in La_2Zn_5Sn and La_2Zn_5Pb

La_2Zn_5Sn			La_2Zn_5Pb		
atom pair	distance (Å)	−*i*COHP (Ry)	atom pair	distance (Å)	−*i*COHP (Ry)
Sn1–Zn2 (2×)	2.713(2)	0.1329	Pb1–Zn2 (2×)	2.756(1)	0.1193
Sn1–Zn3	2.661(2)	0.1628	Pb1–Zn3	2.694(2)	0.1478
Zn1–Zn1	2.582(3)	0.1111	Zn1–Zn1	2.596(3)	0.1079
Zn1–Zn2 (2×)	2.5881(9)	0.1111	Zn1–Zn2 (2×)	2.5834(9)	0.1116
Zn1–Zn2	2.796(2)	0.0846	Zn1–Zn2	2.792(2)	0.0851
Zn2–Zn1 (2×)	2.5881(9)	0.1111	Zn2–Zn1 (2×)	2.5834(9)	0.1116
Zn2–Zn1	2.796(2)	0.0846	Zn2–Zn1	2.792(2)	0.0851
Zn2–Zn3	2.585(2)	0.1121	Zn2–Zn3	2.579(2)	0.1134
Zn3–Zn1 (4×)	2.964(1)	0.0546	Zn3–Zn1 (4×)	2.957(1)	0.0556
Zn3–Zn2 (2×)	2.585(2)	0.1121	Zn3–Zn2 (2×)	2.579(2)	0.1134
La1–Zn1 (4×)	3.185(1)	0.0533	La1–Zn1 (4×)	3.197(1)	0.0506
La1–Zn1 (2×)	3.295(1)	0.0490	La1–Zn1 (2×)	3.306(1)	0.0476
La1–Zn2 (4×)	3.239(1)	0.0514	La1–Zn2 (4×)	3.249(1)	0.0502
La1–Zn2 (2×)	3.345(1)	0.0377	La1–Zn2 (2×)	3.344(1)	0.0365
La1–Zn3	3.210(2)	0.0474	La1–Zn3	3.199(2)	0.0469
La1–Sn1 (2×)	3.385(2)	0.0672	La1–Pb1 (2×)	3.401(2)	0.0618
La2–Zn1 (2×)	3.257(1)	0.0552	La2–Zn1 (2×)	3.276(1)	0.0551
La2–Zn2 (4×)	3.467(1)	0.0400	La2–Zn2 (4×)	3.492(1)	0.0390
La2–Sn1 (4×)	3.3610(5)	0.0775	La2–Pb1 (4×)	3.3660(3)	0.0747

dx.doi.org/10.1021/ic401339v | *Inorg. Chem.* 2013, 52, 9102–9110

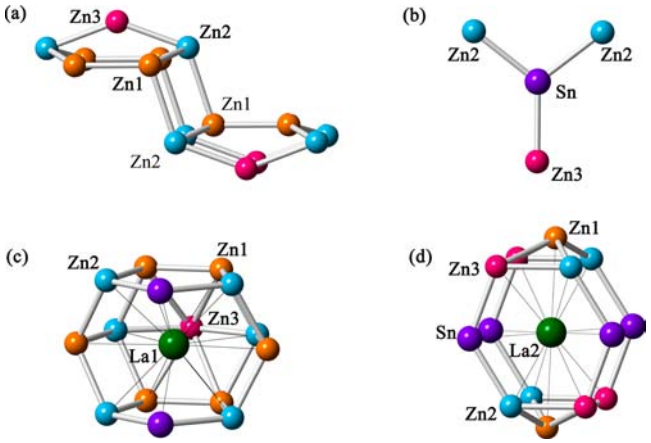

Figure 2. (a) Close view of the zinc "clusters" and the manner in which they are interconnected. Also shown are close views of the local coordination environments of (b) Sn, (c) La1, and (d) La2. La2 is shown with its 10 closest neighbors (<3.5 Å), along with the four Zn3 atoms 3.65 Å away. For all other corresponding distances, the reader is referred to Table 5.

membered Zn_6 rings are capped on the top by another Zn atom (Zn3), forming "Zn_7 cups" with Zn−Zn distances ranging from 2.585(2) Å to 2.964(1) Å in La_2Zn_5Sn, and from 2.579(2) Å to 2.957(1) Å in La_2Zn_5Pb (see Table 5). Notice that the Zn−Zn distances do not appear to correlate in any way with the increased unit-cell volume of La_2Zn_5Pb, compared to that of La_2Zn_5Sn (unlike the La−Zn distances). Also, one should notice that the Zn2−Zn3 bonds, which anchor the Zn_7 fragments into layers, extending in the *ac*-plane, are even longer than the Zn1−Zn2 bonds; the latter measure 2.796(2) Å in La_2Zn_5Sn (2.792(2) Å in La_2Zn_5Pn). For reference, the shorter Zn−Zn contacts are close to the double the radii of the Zn atoms (Pauling covalent radius r_{Zn} = 1.22 Å),[13] while the other ones are substantially longer. The above suggests that there are regions in the Zn substructure with vastly different Zn−Zn bonding. These are known traits of the Zn−Zn interactions in related Zn-rich compounds,[31] such as $NaZn_{13}$,[32] Ce_3Zn_{11},[33] $Na_{34}Zn_{66}Sn_{38}$,[34] and $RE_2Zn_6Ge_3$ (RE = La−Nd),[35] among others. As mentioned in those earlier papers, the Zn−Zn interactions have flexibility, which can lead to the coexistence of two-center, two-electron, and multicenter configurations within the same structure; judging from the Zn−Zn distances, this must also be the case in the RE_2Zn_5Tt (RE = La−Nd; Tt = Sn and Pb) structures.

The Sn and Pb atoms in RE_2Zn_5Tt are found at the centers of trigonal prisms made of rare-earth atoms (see Figure 2b), a building unit that is the hallmark of the AlB_2 structure type.[36] The Zn−Sn and Zn−Pb bonds measure from 2.661(2) Å to 2.713(2) Å, and from 2.694(2) Å to 2.756(1) Å, respectively (see Table 5). These values compare well with the sum of the corresponding Pauling radii ($r_{Zn} + r_{Sn}$ = 2.61 Å; $r_{Zn} + r_{Pb}$ = 2.68 Å)[13] and also match the distances reported for other ternary compounds such as AeZnSn (ZrBeSi structure type),[37] REZnSn,[20a] and CeZnPb (YPtAs structure type),[20b] to name a few. On the basis of the distances, it could be suggested that the bonding interactions between Zn and the tetrel element are most likely covalent in nature.

There are two crystallographic sites for the La atoms, as shown in Figures 2c and 2d. La1 is 15-coordinated and resides within the Zn layers. This atom has 13 next-nearest Zn and 2 next-nearest Sn/Pb atoms (Table 5, cutoff distance 3.5 Å). The La2 atoms have 6 next-nearest Zn and 4 next-nearest Sn/Pb atoms, with 4 additional Zn atoms at ca. 3.65 Å away. Regardless of the lower coordination number of La2 compared to La1, La1 appears to be more tightly coordinated, as judged by the shortest distances to its neighboring atoms. These arguments also support the observation that the isoelectronic substitution of La with a spatially smaller rare-earth element, such as Tm in $LaTmIr_2Ge_4$,[38] will take place, preferably at the La1 site.

A brief comment on some analogous structures is also warranted. The La_2Zn_5Sn structure is closely related to the $EuIn_4$ structure,[8b] which is a monoclinically distorted derivate of the well-known $BaAl_4$ structure type.[4] A schematic

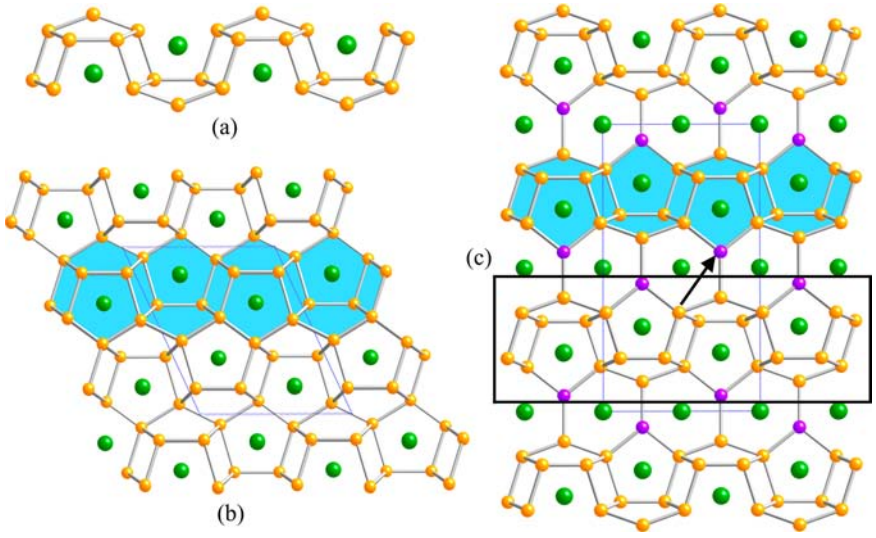

Figure 3. (a) Schematic drawing showing the isolated Zn (colored in orange) layer from the La_2Zn_5Sn structure. (b) Ball-and-stick representation of the monoclinic structure of $EuIn_4$. (c) Ball-and-stick representation of La_2Zn_5Sn. A similar structural fragment is highlighted in light blue to guide the eye. The structural relationship between $EuIn_4$ and La_2Zn_5Sn can be easily recognized by removing the Sn atoms (shown in purple in panel (c)) and moving the next layer (enclosed in the box) in a direction indicated by the arrow.

dx.doi.org/10.1021/ic401339v | *Inorg. Chem.* 2013, 52, 9102−9110

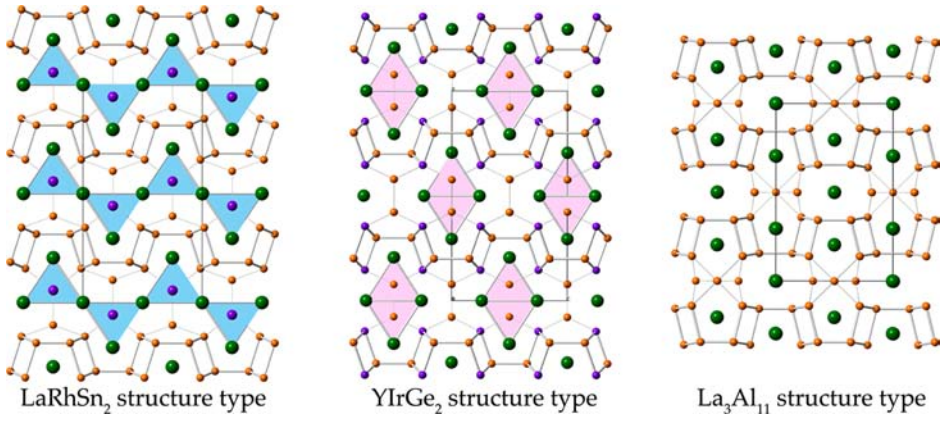

Figure 4. Schematic representations of the $LaRhSn_2$, $YIrGe_2$, and La_3Al_{11} structures types. La_2Zn_5Sn (shown here) and $LaRhSn_2$ are isotypic and the diagram showing them side-by-side is provided as Supporting Information. One immediately notices that in all three structures, similar layers can be found. They are stacked differently, which influences the way rare-earth metal atoms fill the space between the layers.

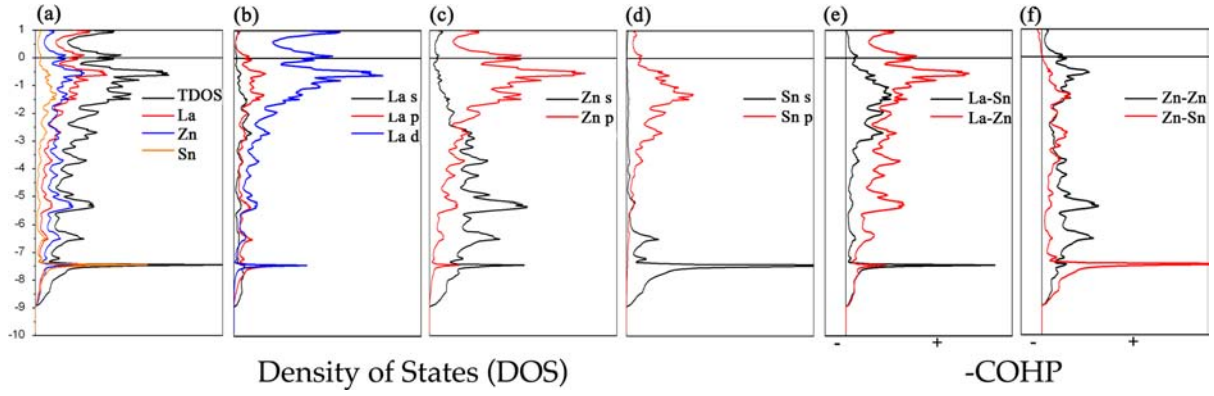

Figure 5. (a) Calculated total density of states (DOS) and partial density of states (PDOS) curves for La_2Zn_5Sn. The Fermi level is the energy reference at 0 eV. The PDOS shows the s, p, and d bands contribution for (b) La, (c) Zn, and (d) Sn. Also shown are the COHP curves for (e) the La−Sn and La−Zn interactions and (f) the Zn−Zn and Zn−Sn interactions. In the −COHP curves, the positive and negative signs represent bonding and antibonding states, respectively.

representation of the structural relationship between $EuIn_4$ and La_2Zn_5Sn is shown in Figure 3. By simply removing the Sn atoms in La_2Zn_5Sn and by shifting the Zn layers in the *b*- and *c*-directions, the topology of the framework of the $EuIn_4$ structure can be obtained. Besides the similarities with $EuIn_4$, we can also draw structural parallels between La_2Zn_5Sn and the La_3Al_{11}[9a] and $YIrGe_2$ structure types.[16] These are shown in Figure 4. As seen from the figure, neighboring Zn layers in La_2Zn_5Sn are not mirror images of each other and the stacking sequence is different than that of the IrGe layers in $YIrGe_2$. For La_3Al_{11}, the layers (without the capping atom) also stack alternately and connect through Al square nets. The "net result" of this is that the manner in which the rare-earth metals fill the space between the layers in each of the three structures is markedly different. For instance, as shown in Figure 4, eight Y atoms encapsulate the Ge_2 dumbbell in AlB_2-like manner (colored in pink) in $YIrGe_2$, while there are only six La atoms in trigonal prismatic fashion (colored in light blue) around the trigonal-planar Sn atom in La_2Zn_5Sn (vide supra). We can speculate that among the most likely reasons for such variations are the crystal packing requirements—Ge has a smaller radius than Sn (r_{Ge} = 1.20 Å, r_{Sn} = 1.29 Å)[13] and the corresponding Ge−Ge distance is significantly shorter than the Zn−Sn distance, which influences what type (i.e., size) of rare-earth atoms can be enclosed between the layers, and ultimately determines their arrangement for most efficient space-filling. Further evidence for this line of thinking is the fact that there are no stannides adopting the $YIrGe_2$ structure type,[16] which also appears to be favored by the late rare-earth metals. In contrast, all the compounds discovered so far with the $LaRhSn_2$ structure type[30] are with the early rare-earth metals and there are no germanides among them. The fact that the series RE_2Zn_5Tt (RE = La−Nd; Tt = Sn and Pb) exist only for the stannide and plumbide analogues, and cannot be extended over Ge or Si, also corroborates this reasoning.

Electronic Structure. In order to understand the chemical bonding, electronic structure calculations of La_2Zn_5Sn and La_2Zn_5Pb were performed using the tight-binding linear muffin-tin orbital (TB-LMTO-ASA) method.[26] The DOS and COHP curves for La_2Zn_5Sn are plotted in Figure 5. As seen from Figure 5a, there is a significant overlap of the valence bands of La, Zn, and Sn throughout the entire energy range, which indicates the strong bonding interactions between all three elements. Figures 5b−d show that, just below the Fermi level, the valence bands arise mainly from the La 5d, Zn 4p, and Sn 5p bands. The 4s and 4p bands of Zn are highly dispersive, whereas the 5s band for Sn (Figure 5d) is highly localized deep below the Fermi level (at ca. −7 eV to −9 eV). This is especially true for the 6s states of Pb in La_2Zn_5Pb, which are found at even lower energy below the Fermi level, as expected for such a heavy element synonymous with the "lone pair" effect. Also, there is insignificant overlapping between the Sn 5s

dx.doi.org/10.1021/ic401339v | Inorg. Chem. 2013, 52, 9102−9110

and 5p bands, and between the Pb 6s and 6p bands, confirming the expected lack of s-p hybridization—again, this is seen very clearly in the case of La_2Zn_5Pb.

No band gaps exist, which is suggestive of the metallic properties of the title compounds. One should also notice that the Fermi level is located slightly above (ca. 0.2 eV) a region with a relatively low DOS (i.e., a pseudo-gap). According to the COHP curves (see Figures 5e and 5f), the bonding interactions at the Fermi level are all in the bonding state, except for the Zn−Sn interactions, which are nearly optimized. The −*i*COHP values in Table 5 indicate that the strongest bonding interactions are indeed the Zn−Sn/Zn−Pb bonds. Regardless of the low content of Sn/Pb in the structure, it appears that the tetrel atoms are critical to its electronic stability. Bonding interactions between La and Zn also exist, albeit weaker, as evident from both the DOS and COHP curves, and they also contribute to the electronic stability of this structure.

On this note, it is useful to compare crystal and electronic structures between the archetype $LaRhSn_2$ and La_2Zn_5Sn in a wider context. First, to rationalize the bonding in both compounds, we invoke the Zintl−Klemm concept[2] as a starting point. Following the rules for simple electron counting, in $LaRhSn_2$, the Sn atoms that are dimerized will require three additional electrons/each to satisfy their octets. Since the Rh atoms do not make any contribution to the magnetization (based on the magnetic susceptibility measurements),[30] a Rh^{3+} with low-spin d^6 electron configuration can be inferred. Hence, the $LaRhSn_2$ formula can be broken down to $[La^{3+}][Rh^{3+}][Sn^{3-}]_2$, and although this idea has already been put forward in a prior publication,[30] we must note that Rh is more electronegative than Sn (χ_{Rh} = 2.2; χ_{Sn} = 1.8).[13] Based on that, considering Rh^{3+} cations alongside Sn^{3-} anions in the same structure is unrealistic, regardless of the seemingly successful application of the Zintl−Klemm concept.[2] The latter approach clearly fails to achieve a meaningful result for La_2Zn_5Sn, with Zn^{2+} and Sn^{4-} being the plausible closed-shell configurations of Zn and Sn (e.g., $[La^{3+}]_2[Zn^{2+}]_5[Sn^{4-}]$).

Arguably, the electron count in La_2Zn_5Sn cannot be straightforward, since the Zn atoms are not involved in simple two-center, two-electron bonds (vide supra). With emphasis on the covalent bonding within the polyanionic framework, then, the La_2Zn_5Sn formula should be best rationalized as $[La^{3+}]_2[Zn_5Sn]^{6-}$, i.e., the Zn atoms will receive some electrons from the La and fill their *p*-orbitals. This is further supported by the fact that, in the result of LMTO calculation, part of the *p*-bands of Zn atoms is indeed below the Fermi level, similar to many other late d-block metals in intermetallics, which receive electrons from the less-electronegative constituents and behave similar to the p-block elements.[39] For $LaRhSn_2$, the electrons provided by the La atoms are not sufficient to fill completely the Rh d-subshell and we should expect major d orbital contribution to the bonding scheme in the polyanionic framework $[RhSn_2]^{3-}$. These differences in the chemical bonding notwithstanding, the valence electron count per formula $LaRhSn_2$ and La_2Zn_5Sn is the same: $LaRhSn_2$ = 3 (La) + 9 (Rh) + 4 (Sn) × 2 = 20, and La_2Zn_5Sn = 3 (La) × 2 + 2 (Zn) × 5 + 4 (Sn) = 20).[40]

Magnetism. The temperature-dependent DC magnetization measurements were performed on samples of RE_2Zn_5Sn (RE = La−Nd) within the temperature range from 5 K to 300 K in field-cooling mode. La_2Zn_5Sn displays a Pauli-like paramagnetic ground state (temperature-independent), as expected for the La^{3+} ion with no 4f electrons. La_2Zn_5Sn is not superconducting at 5 K.

As seen from the Figure 6, the magnetic response for Ce_2Zn_5Sn, Pr_2Zn_5Sn, and Nd_2Zn_5Sn agrees with the local-

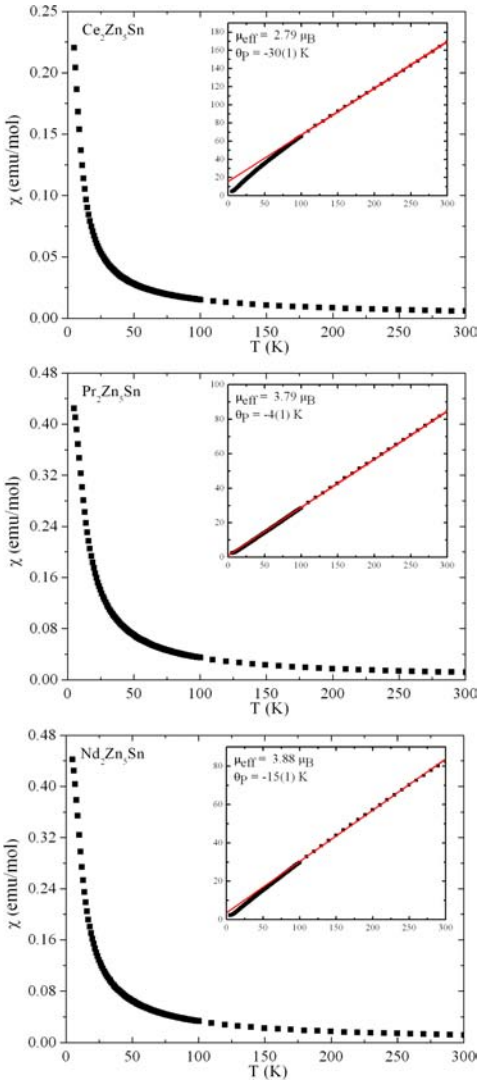

Figure 6. Field-cooled magnetic susceptibility versus temperature of RE_2Zn_5Sn (RE = Ce−Nd). The insets show the temperature dependence of the inverse magnetic susceptibility. The red solid lines are the linear fits of the data, according to the Curie−Weiss law.

moment 4f-magnetism expected for Ce^{3+} ($4f^1$), Pr^{3+} ($4f^2$), and Nd^{3+} ($4f^3$). In the high-temperature regime, all three samples follow the Curie−Weiss law:[41]

$$\chi(T) = \frac{C}{T - \theta_p}$$

where *C* is the Curie constant ($C = N_A\mu_{eff}^2/(3k_B)$) and θ_p is the Weiss temperature. The effective magnetic moments derived from the Curie constants are close to the theoretical values of the free ion RE^{3+}.[41] However, at very low temperatures, the inverse susceptibilities deviate from the linear fits, suggesting the presence of short-range magnetic correlations, although there are no obvious magnetic orderings down to 5 K. The low Weiss constants in this series indicate that the magnetic interactions are weak, which likely is a consequence of the

dx.doi.org/10.1021/ic401339v | Inorg. Chem. 2013, 52, 9102−9110

relatively long RE−RE distances (>4 Å, which is longer than those in the rare-earth elemental form[42]). Attention should be drawn to the fact that, for Ce_2Zn_5Sn, the deviation from the Curie−Weiss behavior occurs at higher temperature than in Pr_2Zn_5Sn and Nd_2Zn_5Sn, which also yields a much higher Weiss constant. This anomaly is not fully understood at the current stage. It may be attributed to a Kondo effect[43] or crystal field splitting of the ground state of the Ce^{3+}.[44] Similar phenomena are also observed in $CeIn_3$,[45] $CeCo_2P_2$,[46] and $CeRhSn_2$.[30]

CONCLUSION

The discovery of the title compounds has again proven the rich "phase space" in these systems, which is worthy of further exploration. Thus, our next target will be the systematic exploration of the RE−Zn−Ge systems (RE = La−Nd), where, until now, we have been unsuccessful in our attempts to synthesize the germanide analogues (RE_2Zn_5Ge). This suggests that there is an intricate interplay between the electronegativity and the atomic sizes in this structure, which warrants further investigation.

ASSOCIATED CONTENT

Supporting Information

A combined X-ray crystallographic file in CIF format. Tables with interatomic distances in RE_2Zn_5Tt (RE = Ce−Nd; Tt = Sn or Pb); a side-by-side structural comparison between La_2Zn_5Sn and $LaRhSn_2$, the DOS and COHP plots for La_2Zn_5Pb, experimental and simulated powder XRD patterns for La_2Zn_5Sn, and view of La_2Zn_5Sn structure with thermal ellipsoids, drawn at the 98% probability level. This material is available free of charge via the Internet at http://pubs.acs.org.

AUTHOR INFORMATION

Corresponding Author

*Tel.: (302) 831 8720. Fax: (302) 831-6335. E-mail: bobev@udel.edu.

Notes

The authors declare no competing financial interest.

ACKNOWLEDGMENTS

The authors gratefully acknowledge the financial support from the National Science Foundation (Grant No. DMR-0743916 (CAREER)).

REFERENCES

(1) (a) Schäfer, H.; Eisenmann, B. *Rev. Inorg. Chem.* **1981**, *3*, 29. (b) Schäfer, H. *Annu. Rev. Mater. Sci.* **1985**, *15*, 1. (c) Nesper, R. *Angew. Chem., Int. Ed.* **1991**, *30*, 789. (d) Westbrook, J. H.; Fleischer, R. L. *Intermetallic Compounds: Principle and Practice*; Wiley: New York, 1995. (e) Kauzlarich, S. M., Ed. *Chemistry, Structure and Bonding of Zintl Phases and Ions*; VCH Publishers: New York, 1996, and the references therein. (f) Guloy, A. M. Polar Intermetallics and Zintl Phases along the Zintl Border. In *Inorganic Chemistry in Focus III*; Wiley−VCH Verlag GmbH & Co. KGaA: Weinheim, Germany, 2006. (g) Corbett, J. D. *Inorg. Chem.* **2000**, *39*, 5178. (h) DiSalvo, F. J. *Pure Appl. Chem.* **2000**, *72*, 1799. (i) Lupu, C.; Downie, C.; Guloy, A. M.; Albright, T. A.; Mao, J.-G. *J. Am. Chem. Soc.* **2004**, *126*, 4386. (j) Corbett, J. D. *Inorg. Chem.* **2010**, *49*, 13.

(2) Zintl, E. *Angew. Chem.* **1939**, *52*, 1.

(3) (a) Bobev, S.; You, T.-S.; Suen, N.-T.; Saha, S.; Greene, R.; Paglione, J. *Inorg. Chem.* **2012**, *51*, 620. (b) You, T.-S.; Tobash, P. H.; Bobev, S. *Inorg. Chem.* **2010**, *49*, 1773.

(4) (a) Andress, K. R.; Alberti, E. *Z. Metallkd.* **1935**, *27*, 126. (b) Ban, Z.; Sikirica, M. *Acta Crystallogr.* **1965**, *18*, 594. (c) Pearson, W. B. *J. Solid State Chem.* **1985**, *56*, 278. (d) Zarechnyuk, O. S.; Kripyakevich, P. I.; Gladyshevskii, E. I. *Sov. Phys. Crystallogr.* **1964**, *9*, 706. (e) Eisenmann, B.; May, N.; Müller, W.; H. Schäfer, H. *Z. Naturforsch.* **1972**, *27b*, 1155.

(5) Zheng, C.; Hoffmann, R. *Z. Naturforsch.* **1986**, *41b*, 292.

(6) Burdett, J. K.; Miller, G. J. *Chem. Mater.* **1990**, *2*, 12.

(7) (a) Häussermann, U.; Amerioun, S.; Eriksson, L.; Lee, C.-S.; Miller, G. J. *J. Am. Chem. Soc.* **2002**, *124*, 4371. (b) Yamanaka, S.; Kajiyama, M.; Sivakumar, S. N.; Fukuoka, H. *High Pressure Res.* **2004**, *24*, 481.

(8) (a) Miller, G. J.; Li, F.; Franzen, H. F. *J. Am. Chem. Soc.* **1993**, *115*, 3739. (b) Fornasini, M. L.; Cirafici, S. *Z. Kristallogr.* **1990**, *190*, 295. (c) Seo, D.-K.; Corbett, J. D. *J. Am. Chem. Soc.* **2000**, *122*, 9621.

(9) (a) Gomes de Mesquita, A. H.; Buschow, K. H. J. *Acta Crystallogr.* **1967**, *22*, 497. (b) Amerioun, S.; Häussermann, U. *Inorg. Chem.* **2003**, *42*, 7782.

(10) Suen, N.-T.; Tobash, P. H.; Bobev, S. *J. Solid State Chem.* **2011**, *184*, 2941.

(11) Tobash, P. H.; Bobev, S.; Thompson, J. D.; Sarrao, J. L. *Inorg. Chem.* **2009**, *48*, 6641.

(12) (a) Solokha, P.; De Negri, S.; Skrobanska, M.; Saccone, A.; Pavlyuk, V.; Proserpio, D. M. *Inorg. Chem.* **2012**, *51*, 207. (b) Suen, N.-T.; Bobev, S. *Eur. J. Inorg. Chem.* **2012**, *26*, 4141.

(13) Pauling, L. *The Nature of the Chemical Bond*, 3rd ed.; Cornell University Press: Ithaca, NY, 1960.

(14) (a) Mishra, T.; Heymann, G.; Huppertz, H.; Pöttgen, R. *Intermetallics* **2012**, *20*, 110. (b) Fritsch, V.; Moreno, N. O.; Thompson, J. D.; Sarrao, J. L.; Bobev, S. *J. Magn. Magn. Mater.* **2006**, *299*, 87. (c) Reker, N.; Johrendt, D.; Pöttgen, R. *Intermetallics* **2013**, *38*, 36.

(15) (a) Kim, S. J.; Kraus, F.; Fässler, T. F. *J. Am. Chem. Soc.* **2009**, *131*, 1469. (b) Kim, S. J.; Hoffman, S. D.; Fässler, T. F. *Angew. Chem., Int. Ed.* **2007**, *46*, 3144.

(16) Francois, M.; Venturini, G.; McRae, E.; Malaman, B.; Roques, B. *J. Less-Common Met.* **1987**, *128*, 249.

(17) Chiotti, P.; Lott, B. G. *Acta Crystallogr.* **1966**, *20*, 733.

(18) Piao, S.; Gómez, C. P.; Lidin, S. *Z. Kristallogr.* **2006**, *221*, 391.

(19) Kripyakevich, P. I.; Kuz'ma, Yu. B.; Ugrin, N. S. *J. Struct. Chem.* **1967**, *8*, 632.

(20) (a) Manfrinetti, P.; Pani, M. *J. Alloys Compd.* **2005**, *393*, 180. (b) Hermes, W.; Rodewald, U. C.; Chevalier, B.; Matar, S. F.; Eyert, V.; Pöttgen, R. *Solid State Sci.* **2010**, *12*, 929.

(21) *SMART NT*, Version 5.63; Bruker Analytical X-ray Systems, Inc.: Madison, WI, 2003.

(22) *SAINT NT*, Version 6.45; Bruker Analytical X-ray Systems, Inc.: Madison, WI, 2003.

(23) Sheldrick, G. M. *SADABS*; University of Göttingen, Göttingen, Germany, 2003.

(24) Sheldrick, G. M. *SHELXTL*; University of Göttingen, Göttingen, Germany, 2001.

(25) (a) Parthé, E.; Gelato, L. M. *Acta Crystallogr., Sect. A: Found. Crystallogr.* **1984**, *A40*, 169. (b) Gelato, L. M.; Parthé, E. *J. Appl. Crystallogr.* **1987**, *20*, 139.

(26) Jepsen, O.; Andersen, O. K. *TB-LMTO-ASAP program*, version 4.7; Max-Planck-Institut für Festkörperforschung, Stuttgart, Germany, 1998.

(27) Dronskowski, R.; Blöchl, P. *J. Phys. Chem.* **1993**, *97*, 8617.

(28) von Barth, U.; Hedin, L. *J. Phys. C: Solid State Phys.* **1972**, *5*, 1629.

(29) Andersen, O. K.; Jepsen, O.; Glötzel, D. *Highlights of Condensed Matter Theory*; Bassani, F., Fumi, F., Tosi, M., Eds.; North−Holland: New York, 1985.

(30) (a) Niepmann, D.; Pöttgen, R.; Küennen, B.; Kotzyba, G.; Rosenhahn, C.; Mosel, B. D. *Chem. Mater.* **1999**, *11*, 1597. (b) Gamża, M.; Ślebarski, A.; Rosner, H. *J. Phys.: Condens. Matter* **2008**, *20*, 025201.

(31) (a) Siegrist, T.; Le Page, Y. *J. Less-Common Met.* **1987**, *127*, 189. (b) Green, M. L. *J. Less-Common Met.* **1973**, *32*, 391. (c) Kuz'ma, Y. B.; Kripyakevich, P. I.; Ugrin, N. S. *Inorg. Mater.* **1966**, *2*, 544.
(32) (a) Zintl, E.; Haucke, W. *Z. Elektrefrochem Angew. Phys. Chem.* **1938**, *44*, 104. (b) Gupta, S.; Corbett, J. D. *Inorg. Chem.* **2012**, *51*, 2247.
(33) Malik, Z.; Sologub, O.; Giester, G.; Rogl, P. *J. Solid State Chem.* **2011**, *184*, 2840.
(34) Kim, S. J.; Fässler, T. F. *J. Solid State Chem.* **2009**, *182*, 778.
(35) Grytsiv, A. V.; Bauer, E.; Berger, S.; Hilscher, G.; Michor, H.; Paul, C.; Rogl, P.; Daoud Aladine, A.; Keller, L.; Roisnel, T.; Noel, H. *J. Phys.: Cond. Matter* **2003**, *15*, 3053.
(36) Hofmann, W.; Jaeniche, W. *Naturwissenschaften* **1935**, *23*, 851.
(37) (a) Iandelli, A. *Rev. Chim. Miner.* **1987**, *24*, 28. (b) Merlo, F.; Pani, M.; Fornasini, M. L. *J. Less-Common Met.* **1991**, *171*, 329.
(38) Malaman, B.; Venturini, G.; Francois, M.; Roques, B. *J. Less-Common Met.* **1989**, *152*, 203.
(39) (a) Whangbo, M.-H.; Lee, C.; Köhler, J. *Angew. Chem., Int. Ed.* **2006**, *45*, 7465. (b) Köhler, J.; Whangbo, M. H. *Chem. Mater.* **2008**, *20*, 2751. (c) Lee, C.; Whangbo, M.-H.; Köhler, J. *Z. Anorg. Allg. Chem.* **2010**, *636*, 36.
(40) Assuming the bonding in La_2Zn_5Sn involves s and p states, and treating the filled d orbitals of Zn as core levels.
(41) (a) Smart, J. S. *Effective Field Theories of Magnetism*; Saunders, Philadelphia, PA, 1966. (b) Kittel, C. *Introduction to Solid State Physics*, 7th ed.; John Wiley and Sons: Hoboken, NJ, 1996.
(42) *Pearson's Handbook of Crystallographic Data for Intermetallic Phases*, 2nd ed.; Villars, P., Calvert, L. D., Eds.; American Society for Metals: Materials Park, OH, 1991.
(43) Kondo, J. *Prog. Theor. Phys.* **1964**, *32*, 37.
(44) Dunn, T. M.; McClure, D. S.; Pearson, R. G. *Some Aspects of Crystal Field Theory*; Harper & Row: New York, 1965.
(45) Buschow, K. H. J.; de Wijn, H. W.; van Diepen, A. M. *J. Chem. Phys.* **1969**, *50*, 137.
(46) Reehuis, M.; Jeitschko, W. *J. Phys. Chem. Solids* **1990**, *51*, 961.

dx.doi.org/10.1021/ic401339v | *Inorg. Chem.* 2013, 52, 9102−9110